3D POST-STACK ONE-WAY MIGRATION USING CURVELETS

BINGBING SUN[1,2], HERVÉ CHAURIS[2,3] and JIANWEI MA[1]

[1] *Institute of Seismic Exploration, School of Aerospace, Tsinghua University, Beijing 100084, P.R. China.*
[2] *Centre de Géosciences, Mines Paristech, 35 rue Saint-Honoré, 77300 Fontainebleau, France.*
[3] *UMR-Sisyphe 7619, France.*

(Received August 17, 2010; revised version accepted June 8, 2011)

ABSTRACT

Sun, B., Chauris, H. and Ma, J., 2011. 3D post-stack one-way migration using curvelets. *Journal of Seismic Exploration*, 20: 257-271.

The classical one-way approximation extrapolates the wavefield from the surface. At each depth level, time shifts are applied in the spatial and wavenumber domains. These shifts are function of the local velocity model. In this paper, following the same strategy as the beamlet migration, we formulate the split-step Fourier method in the curvelet domain. Curvelets are fairly local in the spatial and wavenumber domains, justifying the use of local velocity values in the one-way strategy. In practice, the wavefield is decomposed into 2D curvelets at each extrapolation depth and for fixed frequencies. The derivation is validated through an application on 3D zero-offset migration in a heterogeneous model. This work should be understood as an important step towards a better understanding of the wave propagation in a multi-scale and multi-directional perspective.

KEY WORDS: migration, curvelets, 3D, post-stack.

INTRODUCTION

Seismic imaging consists of retrieving the earth's properties from seismic measurements at the surface. In this paper, we focus on the one-way approximation, where the wavefield is extrapolated in a recursive manner from the surface. Only forward propagation and forward scattering aspects are taken into account, neglecting back-propagation effects. Different methods have been

0963-0651/11/$5.00

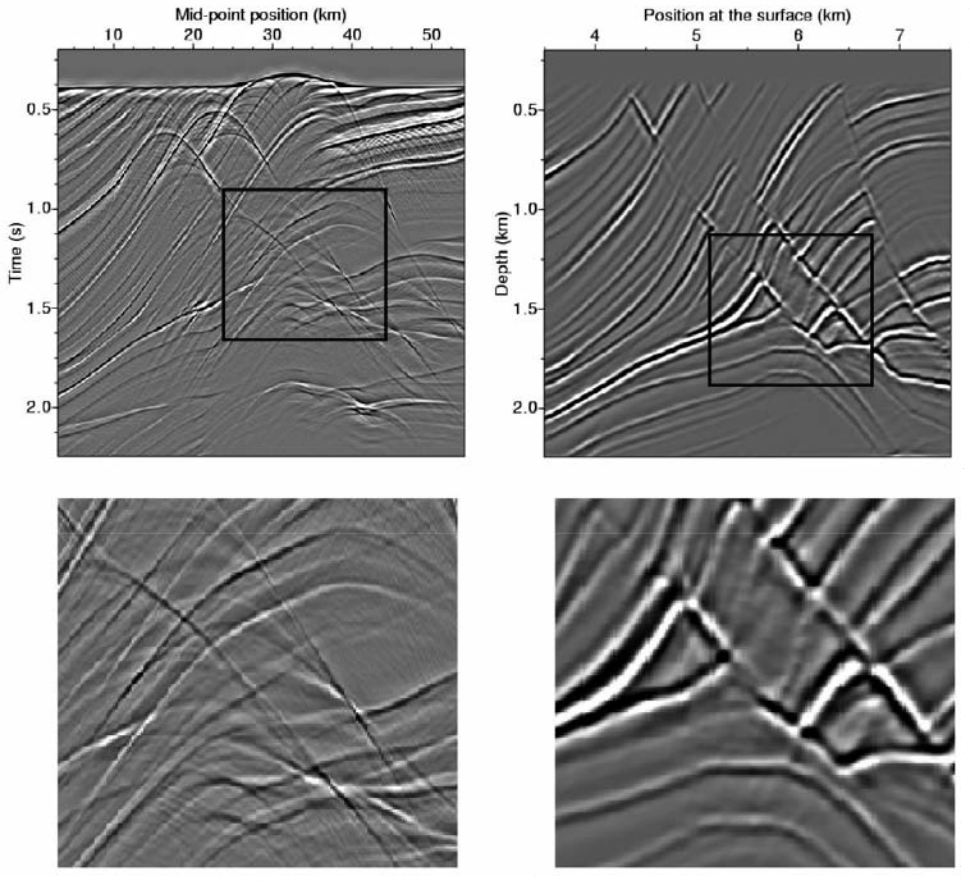

Fig. 1. Top: examples of unmigrated (left) and migrated (right) seismic data. Bottom: zooms of the top figures, underlying the local continuity of seismic events.

developed, depending on the complexity of the velocity model used to simulate the wavefield propagation. We refer to Ferguson (2005) for a complete review. The simplest approach, the classical phase-shift method, extrapolates the wavefield in the wavenumber domain without angle limitations, but is restricted to homogeneous velocity models (Gazdag, 1981). The split-step Fourier method or phase-screen method are designed for weak heterogeneous velocity models (Gazdag and Sguazzero, 1984; Liu and Zhang, 2006; Margrave and Ferguson, 1999). The Generalized-Screen algorithm is valid for strong heterogeneous models (Le Rousseau and de Hoop, 2001). These different approaches rely on both the spatial and wavenumber domains. For classical implementations, the

seismic wavefield has a global extension in one of the two domains: a point-source wavefield is global in the wavenumber domain, whereas a plane wave decomposition is global in the space domain. Due to the large extend of the data, a local approximation of the velocity model to handle heterogeneous models, leads to severe approximations, mainly to angle limitations. For that reason, many authors have proposed alternative decomposition schemes of the wavefield to preserve a local aspect of the data in both the spatial and wavenumber domains.

Seismic data sections generally exhibit local continuity over at least a few traces, both in the unmigrated and migrated domains (Fig. 1). The decomposition of a seismic gather into a sum of local plane waves is thus attractive. We review some existing possibilities characterized by a local extension of the basis functions.

Steinberg (1993) and Steinberg and Birman (1995) developed phase-space propagators based on windowed Fourier transforms (WFTs). Wu and Jin (1997) extended the approach: in their case, the distortion of the wavefield is determined by the local properties of the velocity model. The approach however can be prohibitive in the case of a large number of extrapolation steps due to many applications of the WFTs. Following the same strategy, the beamlet approach proposes two decomposition schemes coupled to the wave propagation: the Gabor-Daubechies frame (GDF) (Wu and Chen, 2001) and the Local Cosine Basis (LCB) (Wu et al., 2008). Beamlets are localized in the spatial and wavenumber domains. The strategy for propagating a wavefield is to locally split the velocity model into two parts: (1) the background velocity model containing the large-scale structure of the model, and (2) the remaining local perturbation. At each propagation step, the wavefield is decomposed in the beamlet domain. Firstly, beamlets are distorted due to a non-homogeneous background model. For smooth models, the high frequency approximation (ray theory) is applicable (Červený, 2001), and Wu et al. (2008) indicated how each beamlet is distorted. Secondly, the rough heterogeneities also affect beamlets. An explicit expression is given under the split-step Fourier approximation, indicating how energy is scattered (Chen et al., 2006).

The objective of this work is to understand if beamlets could be replaced by curvelets, using the same local perturbation strategy to distort the wavefield in heterogeneous models. Curvelets were recently introduced in the field of applied harmonic analysis (Candès et al., 2006), with a number of applications (Herrmann et al., 2008; Ma and Plonka, 2010). This work is motivated by the following properties of curvelets: (1) curvelets are optimal to sparsely represent smooth images with smooth discontinuities; (2) they provide a multi-scale and multi-directional decomposition of the wavefield; (3) curvelets are known to offer a sparse propagation scheme under the high frequency approximation, at least for short-time propagation steps (Candès and Donoho, 2004; Candès and

Demanet, 2005). Both beamlets and curvelets are localized in the space and wavenumber domains. However, curvelets appear to be more elongated than beamlets. More details on the differences between beamlets and curvelets are given in the next section.

Previous publications show attempts to solve the wave equation in the curvelet domain, see for instance Douma and de Hoop (2007); Chauris and Nguyen (2008). They mainly concentrate on the high frequency approximation. In that case, the distortion of a curvelet can be represented by another curvelet, but only for short-time propagation. A more general approach has been proposed by Sun et al. (2009), where the authors derived a simple equation expressing the effect of the Laplacian operator onto a given curvelet. However, these developments are currently limited to homogeneous velocity models. Here, the objective is to derive how curvelets propagate in heterogeneous models under the local perturbation approximation (one-way strategy), to possibly deal with strong velocity contrasts.

The outline of the paper is the following: we first briefly introduce the curvelet construction and indicate the main differences between curvelets and beamlets. We then review the classical split-step Fourier method, and combine it with curvelets. Finally, we demonstrate the applicability on 3D post-stack data before concluding.

CURVELETS

We refer to Candès and Donoho (2004); Candès et al. (2006); Ma and Plonka (2010) for a formal description of curvelets. We only point out here the main properties. A curvelet in 2D is similar to the representation of a local plane wave. Each element can be deduced from a reference curvelet, either by a shift, a rotation or a dilation (Fig. 2).

The curvelet family forms a tight frame: each function $p(\mathbf{x})$ can be expressed as a combination of basis curvelet functions $\varphi_\mu(\mathbf{x})$ [eq. (1)], where $\mathbf{x} = (x,y)$ denotes the spatial coordinates (Candès et al., 2006). The index $\mu = (j,l,k)$ corresponds to the curvelet scale, direction and position. Like for an orthonormal basis, the reconstruction scheme is obtained by

$$p(\mathbf{x}) = \sum_{\mu} c_\mu \varphi_\mu(\mathbf{x}) = \sum_{\mu} <p,\varphi_\mu> \varphi_\mu(\mathbf{x}) \quad . \tag{1}$$

The c_μ value is the curvelet coefficient obtained by the scalar product $<p,\varphi_\mu>$. In practice, the scalar product is obtained in the wavenumber domain (Chauris and Nguyen, 2008)

$$c_\mu = [1/(2\pi)^2] \int \hat{p}(\mathbf{k})\overline{\hat{\varphi}_\mu(\mathbf{k})}d\mathbf{k}$$

$$= [1/(2\pi)^2] \int \hat{p}(\mathbf{k})U_j(S_{\theta_l}\mathbf{k})e^{i<\mathbf{x}_k^{(j,l)},\mathbf{k}>}\, d\mathbf{k} \quad , \tag{2}$$

where $\mathbf{k}$ is the wavenumber associated with $\mathbf{x}$. The function $\hat{\varphi}_\mu$ expresses the curvelet in the 2D wavenumber domain. By construction, it is localized around the central direction of the curvelet (Fig. 3, top). More directions, according to the parabolic scaling, are needed to properly sample the wavenumber domain (Candès et al., 2006). The function S_{θ_l} is the rotation by θ_l radians, indicating the main direction of the curvelet

$$S_{\theta_l} = \begin{pmatrix} \cos\theta_l & \sin\theta_l \\ -\sin\theta_l & \cos\theta_l \end{pmatrix} . \tag{3}$$

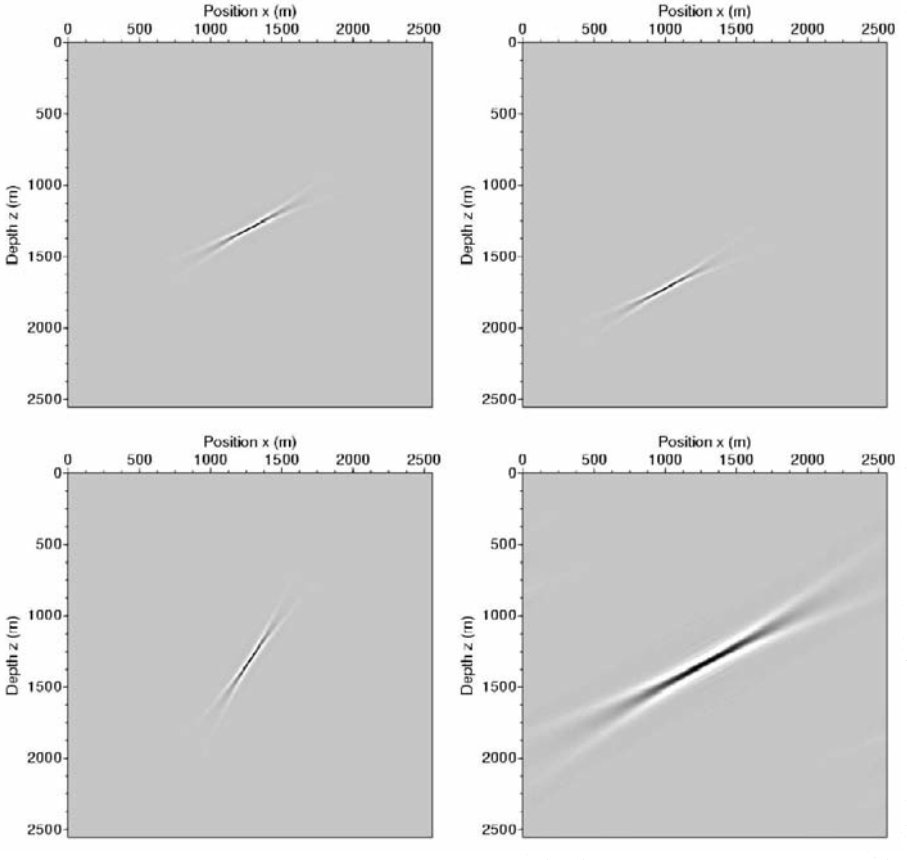

Fig. 2. Reference curvelet (top level) and associated curvelets after shift (top right), rotation (bottom left) and scaling (bottom right).

The filter U_j is constructed as a combination of two functions W(r) and V(θ) defining the radial and angular aspects (Candès et al., 2006; Ma and Plonka, 2010). These window functions are both smooth with W(r) supported on $r \in [1/2,2]$ and V(θ) supported on $[-1,1]$. In the polar coordinates (r,θ), the function U_j is expressed by

$$U_j(r,\theta) = 2^{-3j/4}W(2^{-j}r)V(2^{\lfloor j/2 \rfloor}\theta/2\pi) \quad . \tag{4}$$

The curvelets are both fairly localized in the spatial and wavenumber domains (Fig. 3). The Gabor-Daubechies Frame and Local Cosine Bases beamlets have expressions that differ from the curvelet formula (Chen et al., 2006; Wu et al., 2008). For the Gabor-Daubechies frame beamlet,

$$b_\mu(\mathbf{x}) = g(\mathbf{x} - \mathbf{x}_k)e^{i<\mathbf{x},\mathbf{k}_{j,l}>} \quad , \tag{5}$$

where g is a Gaussian function. The coordinate $\mathbf{k}_{j,l}$ controls the central frequency content and the direction of the beamlet. More details can be found in Chen et al. (2006). Compared to curvelets, beamlets appear to be less elongated (Fig. 3). This is potentially a disadvantage for the wave propagation as with the one-way approximation, the velocity model is locally approximated around a central position. It is thus important to know if curvelets can correctly be propagated in a given velocity model.

WAVE PROPAGATION IN THE CURVELET DOMAIN

Once curvelets have been defined, we first review the split-step Fourier method and show how the wave equation is formulated in the curvelet domain under the one-way approximation.

The split-step Fourier method

Knowing the total wavefield p at a given depth z_n, the objective is to predict the wavefield at the next depth level $z_{n+1} = z_n + \delta z$ for small depth increments. We refer to Stoffa et al. (1990) for more details. The wavefield p is a solution of the seismic wave equation, here the scalar constant density equation expressed in the frequency domain

$$\Delta p(\mathbf{x},z,\omega) + \omega^2 u^2(\mathbf{x},z)p = 0 \quad , \tag{6}$$

where as before $(\mathbf{x},z) = (x,y,z)$ denotes the spatial coordinate, ω the angular frequency and u the slowness field. For simplicity, we did not indicate the source term. The variable z is isolated as a particular coordinate for vertical propagation. Later, the wavefield is thus decomposed in the 2D curvelet domain

(x,y) for fixed depth z and frequency ω. The slowness field is split into two parts, u_0 being a smooth part, and δu a slowness perturbation: $u(\mathbf{x},z) = u_0(z) + \delta u(\mathbf{x},z)$. The split-step Fourier method is summarized in the next equation

$$p(\mathbf{x},z_{n+1},\omega) = e^{iA(\mathbf{x})\delta z}[1/(2\pi)^2] \int \int \hat{p}(\mathbf{k},z_n,\omega)e^{iB(\mathbf{k})\delta z}e^{i<\mathbf{k},\mathbf{x}>}d\mathbf{k} \quad . \tag{7}$$

where $\hat{p}$ is the 2D Fourier transform over $\mathbf{x}$ of p. The square root operator is approximated using the local perturbation theory. It consists of first applying a phase shift in the wavenumber domain, with $B(\mathbf{k}) = \sqrt{(\omega^2 u_0^2 - |\mathbf{k}|^2)}$. The slowness u_0 does not depend on the spatial position. After a 2D inverse Fourier transform, a second phase shift is applied with $A(\mathbf{x}) = \omega\delta u(\mathbf{x})$, to take into account the local velocity perturbation. In practice, the one-way approximation has angle limitations (Stoffa et al., 1990; Ferguson, 2005). The formulation in the curvelet domain consists of decomposing p into a combination of curvelets.

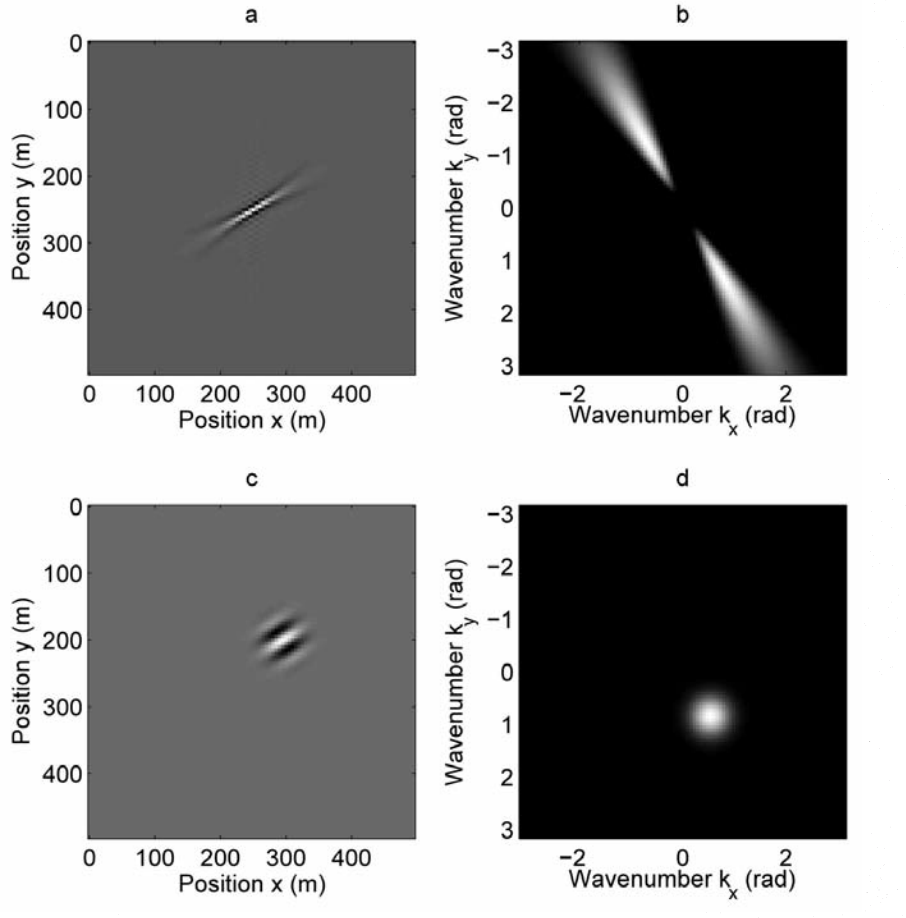

Fig. 3. Curvelet (top) and beamlet (bottom) in the space (left) and wavenumber (right) domains.

Transposition in the curvelet domain

A similar approach is conducted in Wu et al. (2008) for the beamlet case. The wavefields are decomposed into curvelets in the space domain.

$$p(\mathbf{x},z_n,\omega) = \sum_{\mu} c_{\mu}(z_n,\omega)\varphi_{\mu}(x) \quad , \tag{8}$$

$$p(\mathbf{x},z_{n+1},\omega) = \sum_{\mu} c_{\mu}(z_{n+1},\omega)\varphi_{\mu}(x) \quad . \tag{9}$$

The objective is to derive $c_{\mu}(z_{n+1},\omega)$ from $c_{\mu}(z_n,\omega)$. The coefficients are function of the reference depth z_n and the angular frequency ω. Under the split-step Fourier approximation, a single distorted curvelet is expressed as

$$\psi_{\mu}(\mathbf{x}) = e^{iA(x)\delta z}[1/(2\pi)^2] \int \int \hat{\varphi}_{\mu}(\mathbf{k})e^{iB(\mathbf{k})\delta z}e^{i<\mathbf{k},\mathbf{x}>}d\mathbf{k} \quad . \tag{10}$$

The function ψ_{μ} is no longer a strict curvelet. We first decompose the integral on the right into a sum of curvelets $\varphi_{\nu}(\mathbf{x})$ with associated weights $P^0_{\mu,\nu}$ equal to

$$P^0_{\mu,\nu} = \int d\mathbf{x}[1/(2\pi)^2]\varphi_{\mu}(\mathbf{x}) \int \int \hat{\varphi}_{\mu}(\mathbf{k})e^{iB(\mathbf{k})\delta z}e^{i<\mathbf{k},\mathbf{x}>}d\mathbf{k} \tag{11}$$

$$= [1/(2\pi)^2]\varphi_{\mu}(\mathbf{x}) \int \int \hat{\varphi}_{\mu}(\mathbf{k})\hat{\varphi}_{\nu}(-\mathbf{k})e^{iB(\mathbf{k})\delta z}d\mathbf{k} \quad . \tag{12}$$

The modified curvelet is decomposed as

$$\psi_{\mu}(\mathbf{x}) = \sum_{\lambda} P_{\mu,\lambda}\varphi_{\lambda}(\mathbf{x}) \quad , \tag{13}$$

where $P_{\mu,\lambda} = \Sigma_{\nu}P^0_{\mu,\nu}P^1_{\nu,\lambda}$ with

$$P^1_{\nu,\lambda} = \int \int \varphi_{\nu}(\mathbf{x})\varphi_{\lambda}(\mathbf{x})e^{iA(x)\delta z}d\mathbf{x} \quad . \tag{14}$$

The final expression is obtained by

$$c_{\lambda}(z_{n+1},\omega) = \sum P_{\mu,\lambda}c_{\mu} \quad . \tag{15}$$

The operator $P_{\mu,\lambda}$ indicates how curvelets are distorted under the one-way approximation. The two key coefficients $P^0_{\mu,\nu}$ and $P^1_{\nu,\lambda}$ are respectively computed in the wavenumber domain and in the spatial domain, with the appropriate phase

shift corrections. The local perturbation theory is better justified in the case of curvelets thanks to the local aspect of curvelets in the spatial and wavenumber domains.

APPLICATIONS

We test the methodology on a simple impulse response and on a more complex velocity model. In the two cases, the 3D zero-offset data set is generated with a Finite Difference scheme formulated in the time domain (Noble, 1992), using the exploding reflector technique (Lowenthal et al., 1976). We migrate the data in the curvelet domain, under the one-way approximation. It simply consists of summing the wavefield at each spatial location over all frequencies in eq. (9).

The first data set is the impulse response of a homogeneous velocity model at 2 km/s containing a single diffraction point. The model is discretized on a grid of $128 \times 128 \times 128$, using $\Delta x = \Delta y = \Delta z = 10$ m. After migration, the curvelet result nicely compares with the split-step Fourier result (Fig. 4). The curvelet image does not suffer from artifacts due to truncations in the Fourier transform. Furthermore, the curvelet migration takes advantage of the local aspect of the data in the spatial and wavenumber domains.

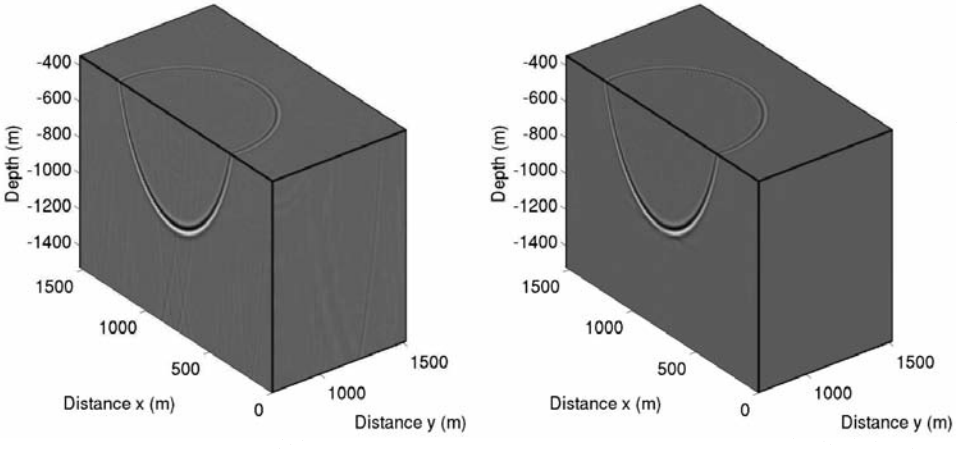

Fig. 4. Impulse responses obtained with the split-step Fourier method (left) and with the curvelet method (right).

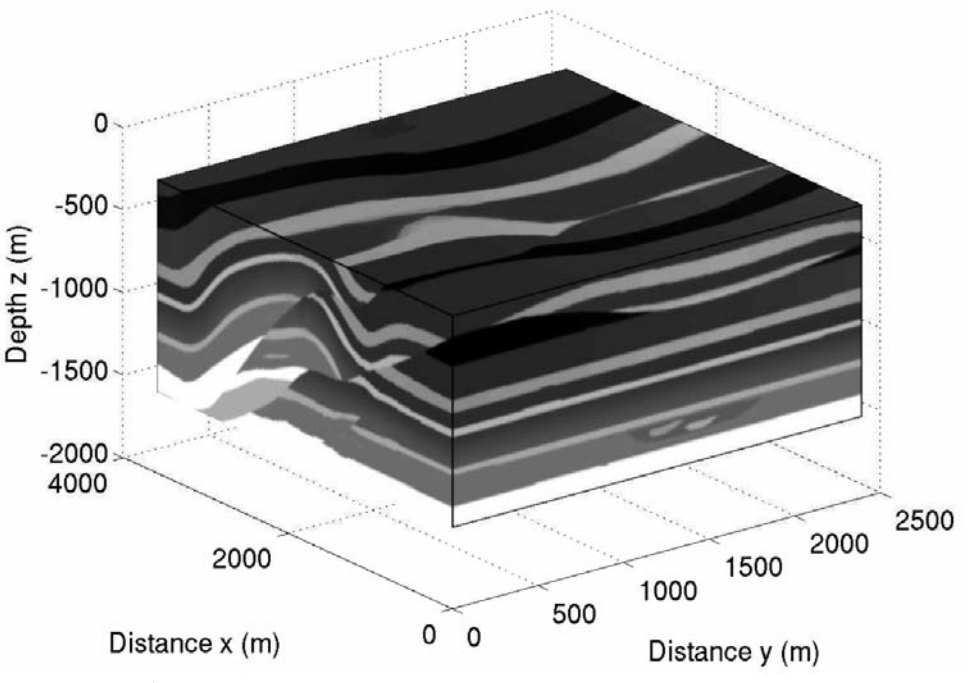

Fig. 5. 3D velocity model used to generate the zero-offset 3D data. The velocity values range from 2 km/s in black to 2.5 km/s in white.

The second data set is built from a modified version of the 3D Overthrust velocity model (Aminzadeh et al., 1997). The velocity values range from 2 km/s to 2.5 km/s (Fig. 5) and is discretized on a grid of 300 $\times$ 200 $\times$ 128 with $\Delta x = \Delta y = \Delta z = 12$ m. The maximum frequency is set to 30 Hz, with a time increment of 2.5 ms (Fig. 6, top). The Finite Difference scheme is of order 4 in time and 8 in space, with 5.5 points per wavelengths to limit the numerical dispersion. After migration, the energy is focused at the position of the interfaces. This demonstrates the ability for curvelets to correctly obtain the migration result under the one-way approximation. The same conclusion holds for the extracted sections for y = 1.2 km (Figs. 7 and 8). However, events with a too small extend are not clearly visible after migration (e.g., on the bottom right for z around 1.3 km and x around 3 km) due to the limited maximum frequency of the input data.

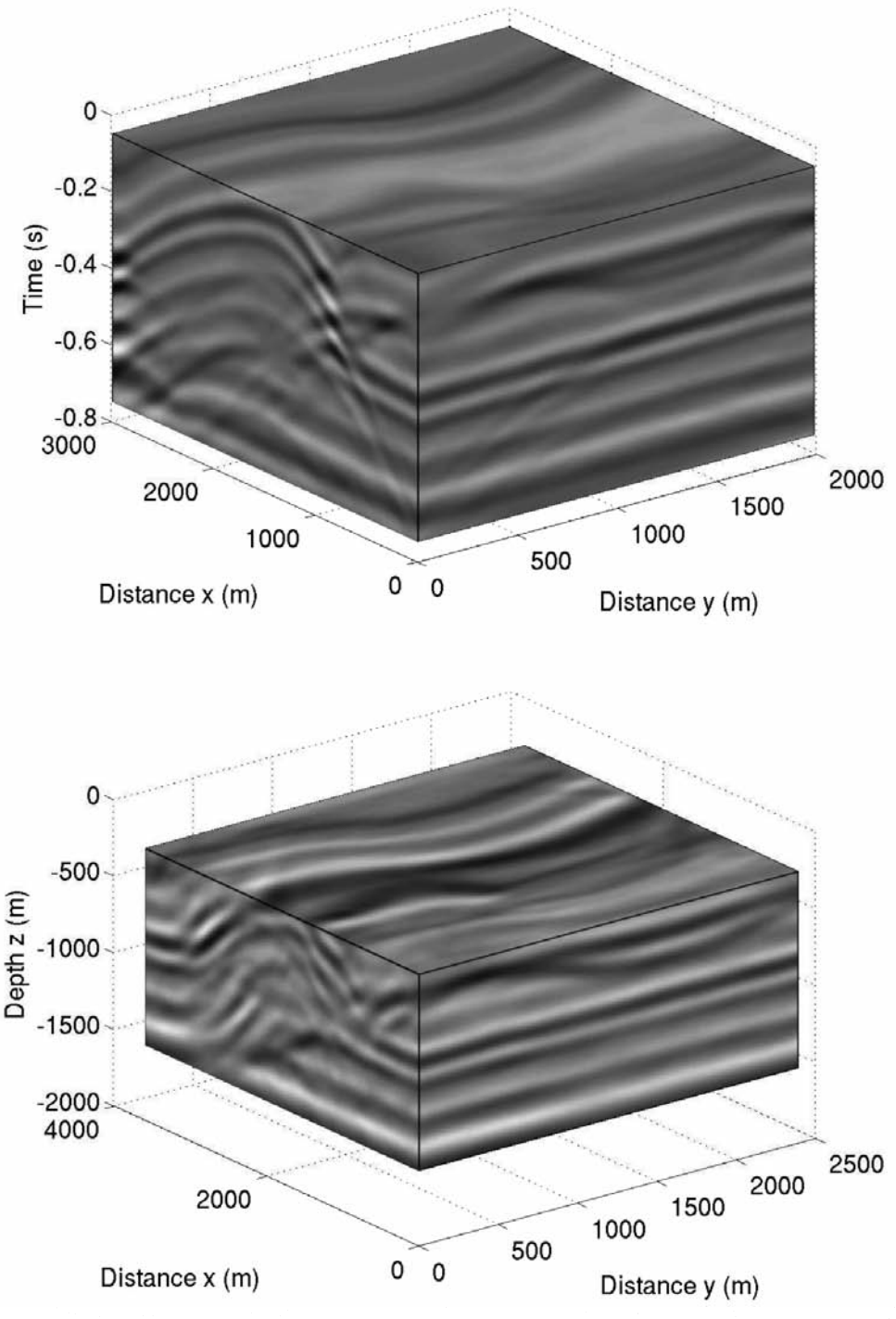

Fig. 6. 3D zero-offset unmigrated input data (top) and associated curvelet migration result (bottom).

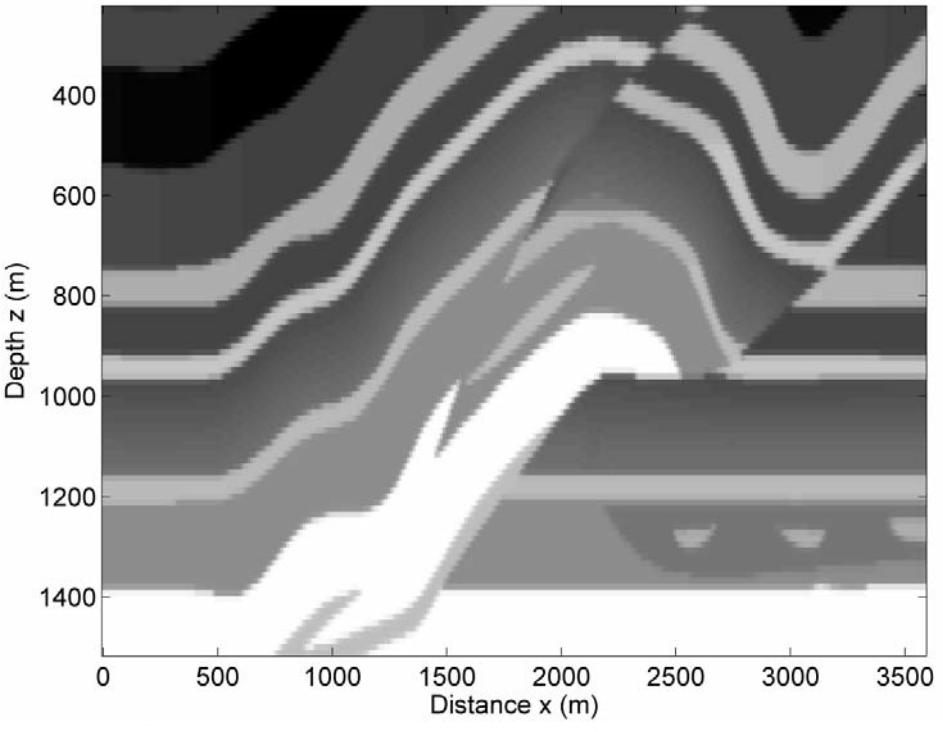

Fig. 7. 2D section for y = 1.2 km, extracted from the velocity model used to generate the zero-offset 3D data. The velocity values range from 2 km/s in black to 2.5 km/s in white.

As mentioned in the introduction section on curvelet, beamlets are less elongated than curvelets. This is potentially an advantage for beamlets, as the split-step Fourier method requires to shift the data in the spatial and wavenumber domains. Despite more elongated shapes, the curvelets are able to focus energy after migration. This offers a large number of possible applications. For each scale and each initial direction, a migrated cube can be computed. The final result can also be decomposed function of the local dip inherent to curvelets. This is for example a way to correct for illumination (Cao and Wu, 2009).

Beamlets however have a significant advantage over curvelets, as they form an orthogonal basis: the scalar product between two different beamlets is equal to zero. This is not the case for curvelets. The curvelet transform is redundant, with a redundancy ratio between 5 to 10, depending on the implementation (Chauris and Nguyen, 2008). More importantly, eqs. (12) and (14) cannot be easily evaluated. It is however possible to restrict the summations over curvelets having a common support. Further investigations should still be conducted to obtain an efficient implementation.

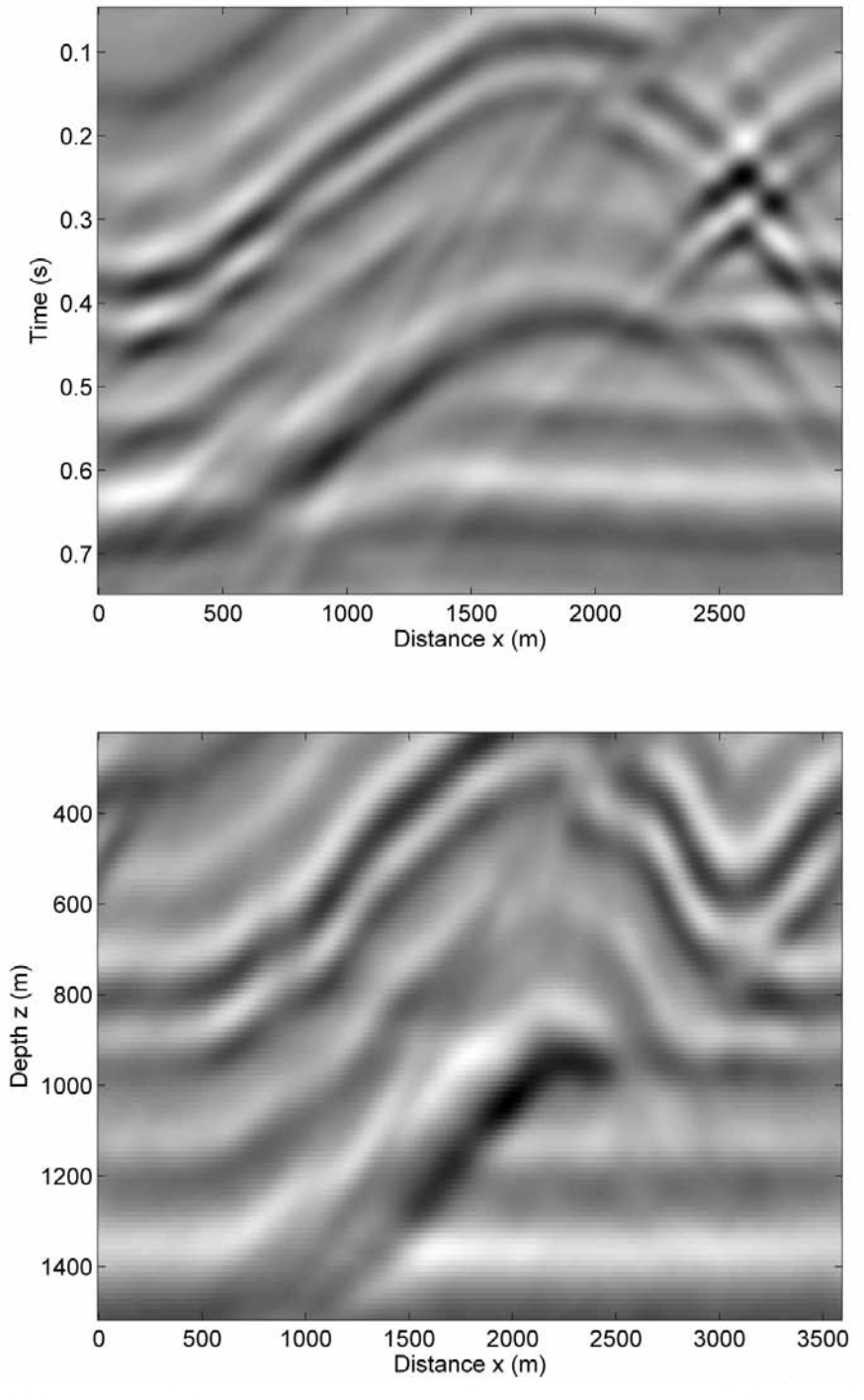

Fig. 8. 2D sections for y = 1.2 km, extracted from the zero-offset unmigrated input data (top) and from the associated curvelet migration result (bottom).

CONCLUSIONS

We have shown how seismic wave propagation and seismic migration can be simulated in the curvelet domain under the one-way approximation. The strategy is similar to the beamlet propagation technique. Compared to the classical split-step Fourier method, the curvelet approach offers the advantage to locally decompose the input data in the spatial and wavenumber domain, justifying the use of the local velocity values. This work should be further evaluated on more models with stronger velocity contrasts. Once an efficient scheme for evaluating the scalar product between two curvelets is obtained, it offers many opportunities to perceive the wave propagation in complex models in a multi-scale and multi-directional approach.

REFERENCES

Aminzadeh, F., Brac, J. and Kunz, T., 1997. 3-D Salt and Overthrust Models. SEG, Tulsa.

Candès, E. and Demanet, L., 2005. The curvelet representation of wave propagators is optimally sparse. Communic. Pure Appl. Mathemat., 58: 1472-1528.

Candès, E., Demanet, L., Donoho, D. and Ying, L., 2006. Fast discrete curvelet transform. SIAM Multiscale Model. Simulat., 5: 861-899.

Candès, E. and Donoho, D., 2004. New tight frames of curvelets and optimal representations of objects with C^2 singularities. Communic. Pure Appl. Mathemat., 57: 219-266.

Cao, J. and Wu, R., 2009. Fast acquisition aperture correction in prestack depth migration using beamlet decomposition. Geophysics, 74: S67-S74.

Červený, V. (Ed.), 2001. Seismic Ray Tracing. Cambridge University Press, Cambridge.

Chauris, H. and Nguyen, T., 2008. Seismic demigration/migration in the curvelet domain. Geophysics, 73: S35-S46.

Chen, L., Wu, R. and Chen, Y., 2006. Target-oriented beamlet migration based on Gabor-Daubechies frame decomposition. Geophysics, 71: S37-S52.

Douma, H. and de Hoop, M.V., 2007. Leading-order seismic imaging using curvelets. Geophysics, 72: S231-S248.

Ferguson, R., 2005. A quantitative comparison of one-way extrapolation operators. J. Seismic Explor., 14: 75-104.

Gazdag, J., 1981. Modeling of the acoustic wave equation with transform methods. Geophysics, 46: 854-859.

Gazdag, J. and Sguazzero, P., 1984. Migration of seismic data by phase shift plus interpolation. Geophysics, 49: 124-131.

Herrmann, F.J., Wang, D. and Verschuur, D.J., 2008. Adaptive curvelet-domain primary-multiple separation. Geophysics, 73: A17-A21.

Le Rousseau, J. and de Hoop, M., 2001. Modeling and imaging with the scalar generalized-screen algorithms in isotropic media. Geophysics, 66: 1551-1568.

Liu, L. and Zhang, J., 2006. 3D wavefield extrapolation with optimum split-step Fourier method. Geophysics, 71: 95-108.

Lowenthal, D., Lu, L., Robertson, R. and Sherwood, J., 1976. The wave equation applied to migration. Geophys. Prosp., 24: 380-399.

Ma, J. and Plonka, G., 2010. The curvelet transform: a review of recent applications. IEEE Signal Proc. Magaz., 27: 118-133.

Margrave, G. and Ferguson, R., 1999. Wavefield extrapolation by nonstationary phase shift. Geophysics, 64: 1067-1078.

Noble, M., 1992. Inversion non linéaire de Données de Prospection Pétrolière. Ph.D. thesis, Université Paris 7, Paris.

Steinberg, B., 1993. Evolution of local spectra in smoothly varying nonhomogeneous environments - local canonization and marching algorithms. J. Acoust. Soc. Am., 93: 2566-2580.

Steinberg, B. and Birman, R., 1995., Phase-space marching algorithm in the presence of a planar wave velocity discontinuity - a qualitative study. J. Acoust. Soc. Am., 98: 484-494.

Stoffa, P.L., Fokkema, J.T., de Luna Freire, R. and Kessinger, W., 1990. Split-step Fourier migration. Geophysics, 55: 410-421.

Sun, B., Ma, J., Chauris, H. and Yang, H., 2009. Solving wave equations in the curvelet domain: a multi-scale and multi-directional approach. J. Seismic Explor., 18: 385-399.

Wu, R. and Chen, L., 2001. Beamlet migration using Gabor-Daubechies frame propagator. Extended Abstr., 63rd EAGE Conf., Amsterdam: 74.

Wu, R., Wang, Y. and Luo, M., 2008. Beamlet migration using local cosine basis. Geophysics, 73: S207-S217.

Wu, R.S. and Jin, S., 1997. Windowed GSP (generalized screen propagators) migration applied to SEG-EAGE salt model data. Expanded Abstr., 67th Ann. Internat. SEG Mtg., Dallas: 937-940.